The synthesis under controlled oxygen partial pressure and the characterization of a layered perovskite system $Sr_2V_{1-x}Mo_xO_4$

2009 J. Phys.: Condens. Matter 21 285601

(http://iopscience.iop.org/0953-8984/21/28/285601)

J. Phys.: Condens. Matter **21** (2009) 285601 (6pp) doi:10.1088/0953-8984/21/28/285601

The synthesis under controlled oxygen partial pressure and the characterization of a layered perovskite system $Sr_2V_{1-x}Mo_xO_4$

Shinji Kouno[1,2], Naoki Shirakawa[1], Yoshiyuki Yoshida[1], Norio Umeyama[1], Kazuyasu Tokiwa[2] and Tsuneo Watanabe[2]

[1] Nanoelectronics Research Institute, Advanced Industrial Science and Technology (AIST), Tsukuba, Ibaraki 305-8568, Japan
[2] Department of Applied Electronics, Tokyo University of Science, Noda, Chiba 278-8510, Japan

E-mail: yoshida.y@aist.go.jp

Received 30 October 2008, in final form 28 April 2009
Published 17 June 2009
Online at stacks.iop.org/JPhysCM/21/285601

Abstract

We have successfully synthesized $Sr_2V_{1-x}Mo_xO_4$ from $x = 0.3$ to 1.0 by an improved process. The layered compound Sr_2VO_4 is an antiferromagnetic insulator with $S = 1/2$, while the isostructural Sr_2MoO_4 is a Pauli paramagnetic metal. The solid solution $Sr_2V_{1-x}Mo_xO_4$ of these materials is expected to show a metal–insulator transition. In this paper we report the synthetic process and the results of the magnetic susceptibility and the electrical resistivity. The selection of the starting materials and the adjustment of O_2 partial pressure of less than 10^{-12} atm were indispensable for the synthesis. The reducing conditions during the sintering had been determined rationally, according to thermodynamical analysis. Kondo-like behavior in both resistivity and magnetic susceptibility were observed in a limited range of V-containing samples.

(Some figures in this article are in colour only in the electronic version)

1. Introduction

Since the discovery of high-transition-temperature (high-T_c) superconductivity in cuprates, a lot of research efforts have been dedicated to the quest for non-cuprate superconductors, in order to better understand the high-T_c phenomenon [1–4]. One of the guiding principles for finding a new superconductor has been the carrier doping of an antiferromagnetic insulator, as it is quite likely that magnetic excitations contribute to the pairing mechanism of high-T_c superconductivity [5]. For instance, a layered compound La_2CuO_4, the mother material of a high-T_c superconductor, transforms, with the hole doping by Sr substitution, from an antiferromagnetic insulator into a superconductor through an abnormal metal with a pseudo-gap [6]. To evaluate the role of antiferromagnetism, it is important to understand the doping and temperature dependence of two-dimensional antiferromagnetic spin fluctuations. Many attempts at carrier doping have therefore been performed on numerous antiferromagnetic insulators (AFI).

Among these AFI there is Sr_2VO_4, which has a similar crystal structure to that of La_2CuO_4 [7]. The compound containing V^{4+} ions has the electron configuration of $3d^1 (S = 1/2)$, in contrast to Cu^{2+} having $3d^9 (S = 1/2)$. In the search for new superconductors, an electron doping by La as a substitute for Sr in Sr_2VO_4 was carried out because of the similarity to the hole doping in cuprate superconductors, but there have been no reports of it being successful for metallic conduction in bulk samples [8, 9]. As a contrast, films of $(Sr, La)_2VO_4$ which reveal metallic conduction have been prepared [10].

We adopted a different approach, namely, substituting Mo for V. Sr_2MoO_4 shows a metallic conductivity and has a tetragonal structure ($I4/mmm$) without a rotation or tilting

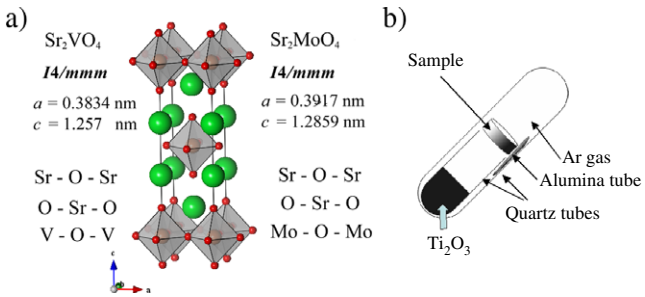

Figure 1. (a) Crystal structure and lattice parameters of layered perovskite $Sr_2(V/Mo)O_4$. The space group of both is $I4/mmm$ within a tetragonal lattice. The layered compounds consist of a perovskite block separated by a rock-salt layer of the composition SrO. V or Mo ions occupy the center of the oxygen octahedron, which has no rotation or tilting. (b) Schematic diagram of the sealed tube for reaction.

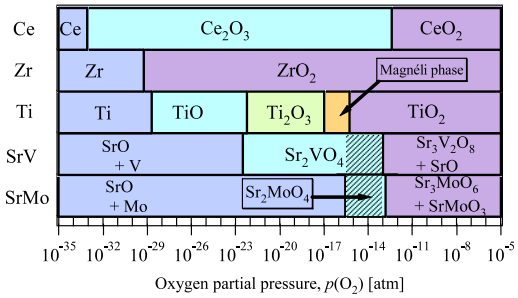

Figure 2. The most stable phase as a function of equilibrium $p(O_2)$ at 1473 K. The hatched area indicates that the $p(O_2)$ range stabilizes both Sr_2VO_4 and Sr_2MoO_4 phases.

of the MoO_6 octahedra as shown in figure 1(a) [11–13]. The transition-metal site substitution, which inevitably disturbs the V–O plane essential for conduction, might be disadvantageous for superconductivity, however, there are encouraging examples of Ba(Pb, Bi)O_3 [14, 15] and La(Fe, Co)AsO [16, 17]. Moreover, there have been few reports on two-dimensional 3d–4d alloy systems with t_{2g} orbitals. A synthesis and characterization of such a system would provide helpful information for further research.

With this in mind, we had to solve a certain problem, that is, the fact that Sr_2VO_4 and Sr_2MoO_4, individually need narrow conditions of a strongly reducing atmosphere upon synthesis. Understandably many researchers had previously reported laborious synthetic methods about these materials [9, 12, 18–23]. Among them, Nozaki *et al* have successfully synthesized the phase-pure polycrystalline sample of Sr_2VO_4 with the aid of TiO as an oxygen getter [18], whereas Shirakawa *et al* have adopted Ti_2O_3 to act as an oxygen buffer in the synthesis of Sr_2MoO_4 [12]. TiO and Ti_2O_3 have different strengths as reduction agents. Shirakawa *et al* qualitatively explained the effect of the oxygen buffer Ti_2O_3 and suggested a practical idea for selecting a suitable buffer for syntheses of some demanding oxides. They have introduced the concept of the ionization tendency of transition-metal ions to stabilize a specific valence.

To extend that concept by Shirakawa *et al*, we have introduced the explicit index of oxygen partial pressure ($p(O_2)$) instead of ionization tendency. This has allowed us to apply a lot of thermochemical data to oxide syntheses. In the present work, we have succeeded in synthesizing the solid solution of $Sr_2V_{1-x}Mo_xO_4$ under controlled $p(O_2)$ based on the thermochemical analysis and have investigated its electrical and magnetic properties. We put particular stress on the explanation of the synthetic process. Moreover, we discuss the difference between the Mo oxides and V oxides in their electrical and magnetic properties.

2. Experimental details

2.1. A selection of the oxygen buffer by thermochemical calculation

We introduced an oxygen buffer in the final calcinations of $Sr_2V_{1-x}Mo_xO_4$ for controlling the $p(O_2)$. This was mandated because that both Sr_2VO_4 and Sr_2MoO_4 are stable phases only within very limited ranges of $p(O_2)$. For example, Lindblom and Rosén reported the equilibrium $p(O_2)$ of Sr_2MoO_4 at 1200 K to be about 10^{-21} atm directly from the experimental results [23]. Yokogawa *et al* showed that Sr_2MoO_4 is the most stable species in the Sr–Mo–O system at 1473 K for the $p(O_2)$ range from 10^{-16} to 10^{-14} atm from their thermodynamic analysis [24].

Now we calculate the most stable phases for both Sr_2VO_4 and Sr_2MoO_4 as a function of $p(O_2)$, following the same thermochemical analysis as performed by Yokogawa above, using the thermodynamical data [25] and the following reaction equations:

$$4Sr_2MoO_4 + O_2 = 2Sr_3MoO_6 + 2SrMoO_3 \quad (1)$$

$$2SrO + Mo + O_2 = Sr_2MoO_4 \quad (2)$$

$$4Sr_2VO_4 + O_2 = 2Sr_3V_2O_8 + 2SrO \quad (3)$$

$$2SrO + V + O_2 = Sr_2VO_4. \quad (4)$$

Figure 2 shows the stable phase relations at 1473 K as a function of $p(O_2)$ for those materials. In addition, Ti, Zr and Ce, which are commonly used as oxygen getters, have been included. Note that we chose the reaction equations such that the valence of the transition metals always increases when going from the left-hand side to the right-hand side. We will be able to stabilize both Sr_2VO_4 and Sr_2MoO_4 in the $p(O_2)$ ranges indicated by the hatched area in figure 2. We expect to be able to prepare the solid solution $Sr_2V_{1-x}Mo_xO_4$ within this area. The equilibrium $p(O_2)$ of Ti_2O_3 becoming TiO_2 through the magnéli phases encompasses around 10^{-16} atm, and this can be used to stabilize both the Sr_2VO_4 and Sr_2MoO_4 phases. On the other hand, the $p(O_2)$ set by the mixture of Ce_2O_3 and CeO_2 is a little higher than the upper bound $p(O_2)$ of Sr_2VO_4, and that set by Zr and ZrO_2 is too low. We have selected, therefore, Ti_2O_3 as the appropriate $p(O_2)$ buffer material.

Table 1. Optimum conditions for syntheses of $Sr_2V_{1-x}Mo_xO_4$. The asterisks indicate that the solid solution was not obtained.

Composition x $Sr_2V_{1-x}Mo_xO_4$	Calcination temperature (K)	Calcination time (h)	Number of intermediate grindings	Buffer's molar ratio y (V, Mo):Ti $= 1:y$
0.1*	1323–1483	160	1–4	Ti_2O_3; 0.5–4.0
0.2*	1323–1483	160	1–4	Ti_2O_3; 0.5–4.0
0.3	1473	100	2	Ti_2O_3; 1.25
0.4	1473	100	3	Ti_2O_3; 1.25
0.5	1473	100	2	Ti_2O_3; 1.0
0.6	1473	100	2	Ti_2O_3; 1.2
0.7	1473	100	2	Ti_2O_3; 1.25
0.8	1473	80	1	Ti_2O_3; 1.3
0.9	1473	80	1	Ti_2O_3; 1.5

2.2. Synthetic procedure

The solid solutions of layered perovskite $Sr_2V_{1-x}Mo_xO_4$ were synthesized from the mixture of both SrO and the precursors of $V_{1-x}Mo_xO_2$ via a conventional solid-state reaction method under the controlled $p(O_2)$ using the oxygen buffer. The precursors were prepared by high-purity VO_2 powder (above 99.9%, Kojundo Chemical Laboratory Co., Ltd) and MoO_2 powder (reagent grade, Soekawa Co., Ltd), and SrO was made by the firing of $SrCO_3$ (99.99%) in air. Then, SrO and the precursor were mixed in the molar ratio of Sr:(V, Mo) = 2:1 and ground in a glove bag filled with N_2 gas. The mixed powder was quickly pressed into a pellet, which was encapsulated in a quartz tube with Ti_2O_3 as the buffer material. The quartz tube consisted of both an outer tube and an inner tube. The powder of Ti_2O_3 was held in the inner 'test tube' made of quartz, and the pellet was set on top of it to prevent the pellet from being contaminated with Ti_2O_3. In order to avoid direct contact between the pellet and the outer quartz tube, it was necessary to place the pellet inside an open alumina tube as shown in figure 1(b). The outer tube with the above contents was first evacuated with a diffusion pump and then charged with Ar gas so that the pressure was going to be 1 atm at the calcination temperature. The outer quartz tube was sealed by fusion, followed by firing in a resistance furnace. The final sample was obtained after several repetitions of firing with intermediate re-grindings and adjusting the amount of the oxygen buffer. The synthetic conditions for each of the solid solutions are shown in table 1.

It became easier to synthesize high-purity samples as we approached the Mo end. In contrast, towards the V end, the samples tended to contain multiple phases; the orthorhombic Sr_2VO_4, not of the K_2NiF_4 type, appeared and grew in volume fraction with an increased amount of the oxygen buffer. With a smaller amount of the oxygen buffer, however, we had instead $Sr_3V_2O_8$ impurity as a secondary phase and we could not find the right amount of the oxygen buffer to eliminate them both. Accordingly, both $Sr_2V_{0.9}Mo_{0.1}O_4$ and $Sr_2V_{0.8}Mo_{0.2}O_4$ contained a significant amount of impurity. Moreover, repetitive intermediate grindings and firings resulted in a separation of Sr_2VO_4 and Sr_2MoO_4 in these low V-concentration samples.

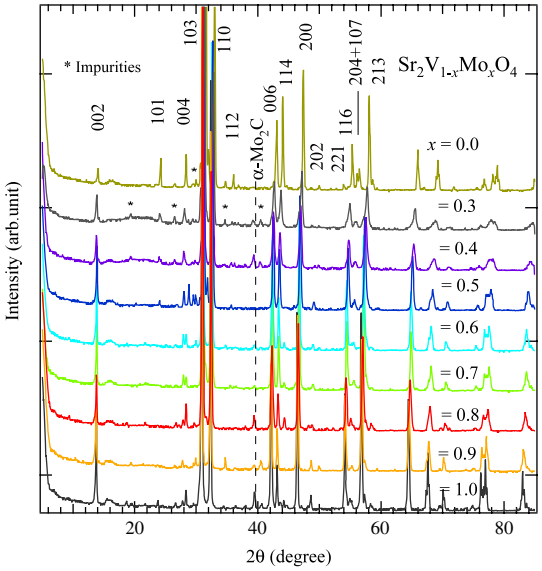

Figure 3. XRD patterns of $Sr_2V_{1-x}Mo_xO_4$. The strongest peak of α-Mo_2C at 39.54° is indicated by the vertical dashed line. The asterisks show the peaks of the impurity phases.

2.3. Characterization of the samples

Powder x-ray diffraction was performed at each synthesis step with Cu Kα radiation at room temperature. Electrical resistivity measurements were performed in the temperature range from 30 mK to 300 K with a dilution refrigerator, using an AC four-probe method. Gold leads were attached to the rectangular shaped bars with silver paint. Magnetization measurements were carried out on a Quantum Design $MPMS_2$ magnetometer in a temperature range of 1.8–300 K on irregularly shaped sintered pellets weighing about 30 mg. Zero-field cooled (ZFC) and field cooled (FC) measurements were performed in a magnetic field $H = 10$ kOe. The sample of $x = 0.8$ was measured also at 10 Oe to check the superconducting volume fraction.

3. Result and discussion

3.1. XRD patterns

Figure 3 represents the powder XRD pattern for all $Sr_2V_{1-x}Mo_xO_4$ studied. All the samples were sufficiently

Table 2. Physical properties of $Sr_2V_{1-x}Mo_xO_4$. The magnetic susceptibilities have been fitted to the Curie–Weiss law, $\chi = \chi_0 + C/(T - \theta_p)$, where χ_0 is the temperature-independent paramagnetism, C the Curie constant and θ_p the Weiss temperature.

	Lattice constants							
Composition x	a (Å)	c (Å)	$\rho_{290\ K}$ (mΩ cm)	χ_0 (emu mol^{-1} × 10^{-4})	C (emu K^{-1} mol^{-1})	θ_p (K)	Average effective moment (μ_B)	Effective moment per V ion (μ_B)
0.3	3.855	12.70	1000	0.90	0.2347	8.4	1.37	1.64
0.4	3.862	12.74	290	1.54	0.2256	0.7	1.34	1.73
0.5	3.876	12.75	49	2.87	0.1464	−50	1.08	1.53
0.6	3.885	12.77	61	3.01	0.1234	−59	0.99	1.57
0.7	3.889	12.79	11	3.54	0.0948	−79	0.87	1.59
0.8	3.896	12.81	40	3.26	0.0566	−67	0.67	1.50
0.9	3.904	12.83	20	2.88	0.0098		0.28	0.88
1.0	3.9168	12.859	9	1.99				

good in the sense of having little impurity phase. Samples with high Mo content, however, tend to include α-Mo_2C as an impurity. The origin of the carbon giving α-Mo_2C is supposedly the starting material of $SrCO_3$ or the oil of the diffusion pump. Apart from this, we were unable to obtain the Mo-substituted samples with x up to 0.3.

For the sample of $x = 0.5$, there are several peaks near 28°. One of the peaks is likely to be from the (004) reflection. The simulation of the XRD pattern for the layer-by-layer stacking of Sr_2VO_4 and Sr_2MoO_4 predicts two strong peaks and several weak peaks near 28°, quite consistent with the observation. The rock-salt type ordering of the B-sites within the plane is unlikely, because it should have peaks at 21° and 18°. $Sr_3V_2O_8$ does have the strongest peak at 28°, but it also has the second strongest at 32°, which is not observed. There are no other known materials that match these peaks.

We indexed, therefore, all the XRD patterns in a body-centered tetragonal space group $I4/mmm$ except for the peaks near 28° and the very small peaks of obvious impurities. We show the lattice parameters of both a and c for various compositions x in figure 4. From $x = 0.3$ to 1.0, both the parameters increase monotonically in line with the Vegard's law, whereas there is no change below $x = 0.3$. This means that the substitution of Mo ions for V has been accomplished in $Sr_2V_{1-x}Mo_xO_4$ for $x = 0.3$ from 1.0.

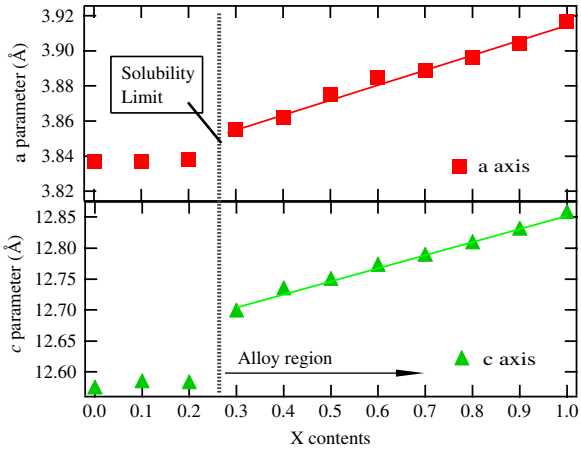

Figure 4. Crystal lattice parameters a and c as functions of the composition x for the polycrystalline $Sr_2V_{1-x}Mo_xO_4$.

3.2. Electrical resistivity

The temperature dependencies of the electrical resistivity between 30 mK and 300 K are shown in figure 5. The resistivities of $Sr_2V_{1-x}Mo_xO_4$ at room temperature, by and large, had a tendency to decrease with the increasing composition x. Non-metallic behavior or low-temperature upturn was observed for $x = 0.3$–0.8. We could not observe a complete superconducting transition in any composition. A small drop was observed for the $x = 0.8$ sample at around 4 K, which coincides with the diamagnetic signal in the small-field ($H = 10$ Oe) susceptibility. But this diamagnetism is as small as 1% of perfect diamagnetism and may well be explained by the presence of α-Mo_2C in the sample.

3.3. Magnetic susceptibility

The temperature dependencies of the magnetic susceptibility between 2 and 300 K are shown in figure 6. The magnetic behavior of $Sr_2V_{1-x}Mo_xO_4$ gradually changed from the Curie–Weiss paramagnetic type at $x = 0.3$ to the Pauli paramagnetic type at the Mo end ($x = 1.0$). Moreover, an anomaly which looked like a spin glass transition previously reported for Sr_2VO_4 [19] was observed around 8 K for $x = 0.3$ and 0.4 in V-rich compositions.

3.4. Discussion

In table 2, some physical parameters of $Sr_2V_{1-x}Mo_xO_4$, based on the above measurements, are summarized, where C is the Curie constant, θ_p the Weiss temperature, and χ_0 the temperature-independent paramagnetism. Since polycrystalline samples cannot give absolute values of electrical resistivity due to the effect of grain boundaries and the mixing of in-plane and out-of-plane conductions in their two-dimensional crystal structure, we focus only on the temperature dependence.

The resistivity behavior over the entire substitutional range shows a crossover from metallic on the Mo end to insulating on the V end. This may be viewed as a composition-induced metal–insulator transition in which electron–electron interaction plays an essential role. However, if we note that we could not alloy Mo with insulating Sr_2VO_4, while metallic Sr_2MoO_4 could accommodate a considerable portion of V

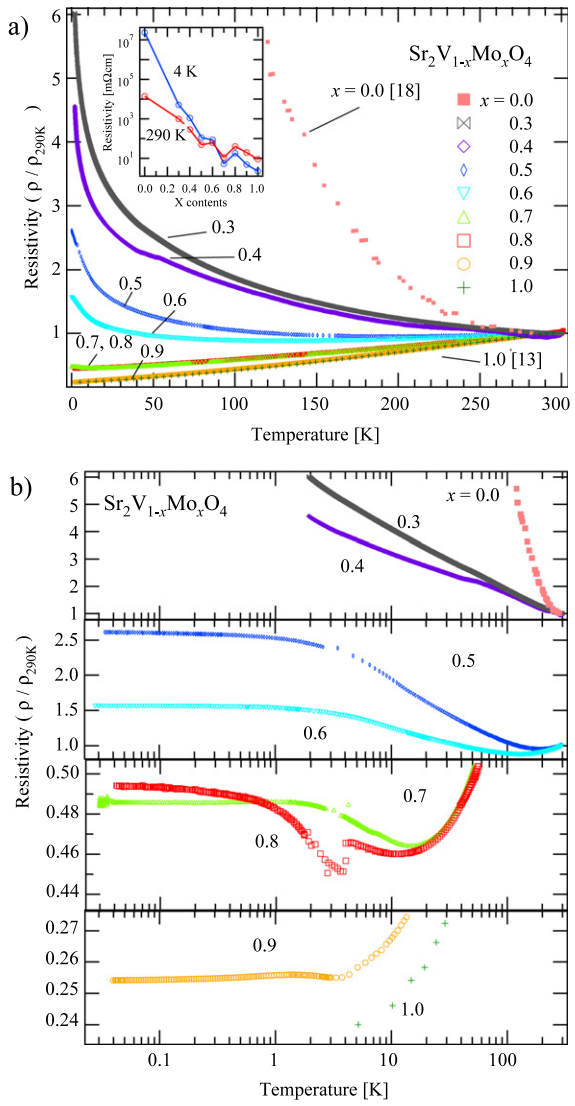

Figure 5. The temperature dependencies of the electrical resistivity of $Sr_2V_{1-x}Mo_xO_4$ between 30 mK and 300 K, scaled at 300 K. See text for the drop around 4 K in the $x = 0.8$ curve.

ion, another interpretation (a Kondo scenario) would also be possible as discussed below.

Figure 5(b) shows that the increase of the resistivities towards low temperature behaves as $\log T$, followed by a saturation. The magnetic susceptibilities deviate from the Curie–Weiss behavior and also show a subsequent saturating trend (the inset of figure 6). These are reminiscent of the Kondo effect in dilute magnetic alloys.

Interestingly, the composition range where this Kondo-like behavior manifests itself nearly coincides with that where the effective moment per V^{4+} ion is almost identical to the spin-only free-ion value of 1.73 μ_B. The difference between what we observe here and the ordinarily dilute magnetic alloys like Cu–Fe is that in the latter the Fe-concentration-independent magnetic moment is established immediately upon doping as low as 50 ppm and the resistance minimum appears [26, 27].

In the present case, however, the Kondo-like behaviors seem to appear only after the effective moment has fully grown

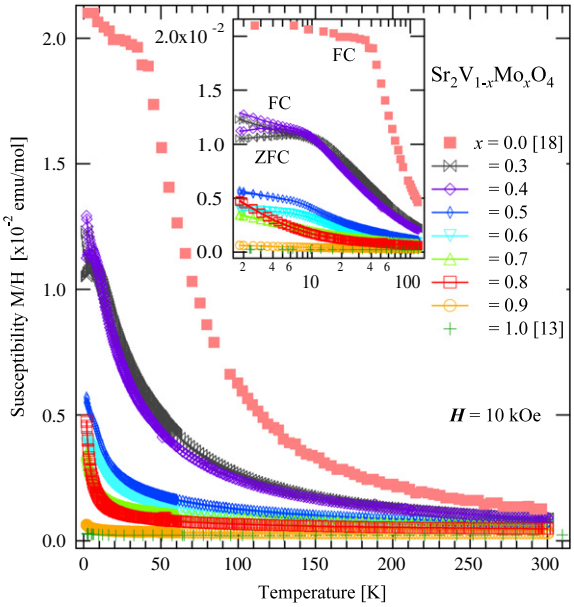

Figure 6. DC magnetic susceptibility of $Sr_2V_{1-x}Mo_xO_4$ between 1.8 and 300 K, for $x = 0.3$–0.9. Inset: a blowup of the data below 30 K, plotted against log T.

to its spin-only value. In oxygen depleted $CaVO_{3-\delta}$ the local magnetic moment induced by oxygen deficiency does not bring about any Kondo effect [28]. Thus in these relatively complex oxide systems the criteria that the local magnetic moments can induce the Kondo effect seem rather limited and in the $Sr_2(V, Mo)O_4$ system the establishment of the full effective moment is the key factor.

In summary, we have described how to synthesize some oxides in well-defined low-$p(O_2)$ ambients on sintering, and that it is possible to choose an O_2 buffer material rationally, based on thermodynamical analysis using the database. This allowed us to prepare the solid solution $Sr_2V_{1-x}Mo_xO_4$, and we succeeded in investigating the physical properties of these oxides with electrical resistivity and magnetic susceptibility. Kondo-like behaviors both in resistivity and magnetic susceptibility were observed in V-containing samples.

Acknowledgments

We would like to thank T Yanagisawa, K Iwata, S Hara and S Koikegami for their support and advice. This research was financially supported by the Sasakawa Scientific Research Grant from the Japan Science Society.

References

[1] Mackenzie A P and Maeno Y 2003 *Rev. Mod. Phys.* **75** 657
[2] Nagamatsu J, Nakagawa N, Muranaka T, Zenitani Y and Akimitsu J 2001 *Nature* **410** 63–4
[3] Yonezawa S, Muraoka Y, Matsushita Y and Hiroi Z 2004 *J. Phys.: Condens. Matter* **16** L9–12
[4] Kamihara Y, Watanabe T, Hirano M and Hosono H 2008 *J. Am. Chem. Soc.* **130** 3296

[5] Lee P A, Nagaosa N and Wen X G 2006 *Rev. Mod. Phys.* **78** 17
[6] Keimer B, Belk N, Birgeneau R J, Cassanho A, Chen C Y, Greven M, Kastner M A, Aharony A, Endoh Y, Erwin R W and Shirane G 1992 *Phys. Rev.* B **46** 14034
[7] Cyrot M, Andron B L, Soubeyroux J L, Rey M J, Dehauht Ph, Lackmann F C, Fourcaudot G, Beille J and Tholence J L 1990 *J. Solid State Chem.* **85** 321–5
[8] Deslandes F, Nazzal A I and Torrance J B 1991 *Physica* C **179** 85–90
[9] Nedilko S A and Drozd V A 2001 *Mater. Lett.* **49** 340–4
[10] Matsuno J, Okimoto Y, Kawasaki M and Tokura Y 2003 *Appl. Phys. Lett.* **82** 194
[11] Shirakawa N and Ikeda S I 2001 *Physica* C **364/365** 309–12
[12] Shirakawa N, Ikeda S I, Matsuhata H and Bando H 2001 *Japan. J. Appl. Phys.* **40** L741–3
[13] Ikeda S I, Shirakawa N, Bando H and Ootuka Y 2000 *J. Phys. Soc. Japan* **69** 3162–5
[14] Sleight A W, Gillson J L and Bielstedt F E 1975 *Solid State Commun.* **61** 27
[15] Tanh T D, Koma A and Tanaka S 1980 *Appl. Phys.* **22** 205
[16] Sefat A S, Huq A, McGuire M A, Jin R, Sales B C, Mandrus D, Cranswick L M D, Stephens P W and Stone K H 2008 arXiv:0807.0823 [cond-mat]
[17] Cao G, Wang C, Zhu Z, Jiang S, Luo Y, Chi S, Ren Z, Tao Q, Wang Y and Xu Z 2008 arXiv:0807.1304 [cond-mat]
[18] Nozaki A, Yoshikawa H, Wada T, Yamauchi H and Tanaka S 1991 *Phys. Rev.* B **43** 181
[19] Suzuki N, Noritake T and Hioki T 1992 *Mater. Res. Bull.* **27** 1171–84
[20] Giannakopoulou V, Odier P, Bassat J M and Loup J P 1995 *Solid State Commun.* **93** 579–83
[21] Itoh M, Shikano M, Kawaji H and Nakamura T 1991 *Solid State Commun.* **80** 545–8
[22] Steiner U and Reichelt W 1998 *Z. Naturf.* b **53** 110–6
[23] Lindblom B and Rosén E 1986 *Acta Chem. Scand.* A **40** 452
[24] Yokogawa H, Sakai N, Kawada T and Dokiya M 1991 *J. Solid State Chem.* **94** 106
[25] *HSC Chemistry* 2002 Outokumpu Research Oy
[26] Hurd C M 1967 *Phys. Rev. Lett.* **18** 1127
[27] Pearson W B 1955 *Phil. Mag. 7* **6** 911
[28] Shirakawa N, Murata K, Makino H, Iga F and Nishihara Y 1995 *J. Phys. Soc. Japan* **64** 4824